Nano Energy 88 (2021) 106308

Contents lists available at ScienceDirect

Nano Energy

journal homepage: www.elsevier.com/locate/nanoen

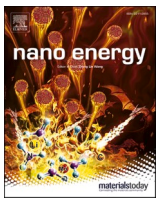

Full paper

Adjustable electrochemical properties of solid-solution MXenes

Likui Wang [a,b,1], Meikang Han [a,1], Christopher E. Shuck [a], Xuehang Wang [a], Yury Gogotsi [a,*]

[a] A.J. Drexel Nanomaterials Institute and Department of Materials Science and Engineering, Drexel University, Philadelphia, PA 19104, United States
[b] International Joint Research Center for Photoresponsive Molecules and Materials, School of Chemical and Materials Engineering, Jiangnan University, Wuxi 214122, China

ARTICLE INFO

Keywords:
MXene
Solid solution
Supercapacitor
Titanium niobium carbide
Vanadium niobium carbide

ABSTRACT

MXenes are promising pseudocapacitive materials with ultrahigh specific capacitance. Currently, more than 30 stoichiometric MXene compositions and about 20 solid solutions have been experimentally synthesized. However, most studies focus on $Ti_3C_2T_x$ or a few other single-M MXenes, and little is known about the electrochemical properties of solid-solution MXenes. Herein, two sets of niobium-based solid-solution MXenes ($Ti_{2-y}Nb_yT_x$ and $V_{2-y}Nb_yT_x$; $0 \leq y \leq 2$) were synthesized and the dependence of their electrochemical properties on the ratio of M elements in the structure was investigated. Relationships between the chemistry and charge storage ability, including capacitive properties and cycling stability in aqueous protic electrolyte, were determined. There is an inverse relationship between the prominence of the redox peaks and cycling stability; the latter increases with the niobium content. For instance, the capacitance retention after 20,000 cycles is less than 1% for Ti_2CT_x, but 78% for $Ti_{0.4}Nb_{1.6}CT_x$. This study shows that electrochemical properties of MXenes can be controlled by tuning the ratio of transition metals in the MXene structure.

1. Introduction

The rapid development of portable electronics and electrical vehicles has led to accelerating demand for battery alternatives that have fast charging rates and long-life spans. Supercapacitors, typically electrochemical double layer capacitors (EDLCs), can be fully charged and discharged in minutes with excellent cyclability [1–4]. In contrast to batteries, which store energy through Faradaic reactions, EDLCs stores charge through physisorption of ions on the surface of porous carbonaceous electrode materials. Their energy density is limited by the accessible surface area, and is lower than batteries. Pseudocapacitive materials store energy through fast and reversible surface redox reactions, providing increased energy storage capability compared to EDLCs. RuO_2 [5–7], MnO_2 [8], Nb_2O_5 [9,10], transition metal nitrides [11–14], and conductive polymers have shown intrinsic pseudocapacitive behavior with fast surface redox reactions [15–17]. However, except for RuO_2 and some of the transition metal nitrides, most pseudocapacitive materials have low electrical conductivities, limiting their power density and cycling performance [18]. High conductivity is of critical importance for fast charging, when high current must flow through the device, and it allows to minimize energy losses related to Joule heating.

MXenes are a class of two-dimensional (2D) transition metal carbides, nitrides, and carbonitrides, which are typically synthesized by selectively etching the A element from $M_{n+1}AX_n$ phases, where M represents early transition metal (Ti, Nb, Mo, V, Cr, Ta, *etc.*), A is a group 13–15 element (Al, Si, Ga, In, *etc.*), X is carbon and/or nitrogen, and n is 1–4 [17,19–21]. After etching, MXenes have the general formula $M_{n+1}X_nT_x$, where T_x represents the surface functional groups (-F, =O, -Cl, -OH, *etc.*) [17,20]. The compositional variety, variable transition metal redox chemistry, scalability, and 2D morphology render MXenes particularly attractive for energy storage applications [17,22–24]. MXenes can contain a single early transition metal or multiple metals in its M layers [25,26]. Furthermore, based on the distribution of the metal atoms, double-metal MXenes include solid-solution MXenes, where the two metal atoms are randomly distributed in M-site, as well as in- and out-of-plane ordered MXenes [27–29].

$Ti_3C_2T_x$ is the first discovered and the most studied MXene, showing the highest reported electrical conductivity (>15,000 S/cm), redox active surface for protonation and good packing density (up to 4 g/cm^3 in stacked films), resulting in volumetric capacitance of 1500 F/cm^3 and high-rate performance in thin films [30,31]. Other MXenes have also

* Corresponding author.
E-mail address: gogotsi@drexel.edu (Y. Gogotsi).
[1] These authors contribute equally to this work.

https://doi.org/10.1016/j.nanoen.2021.106308
Received 24 March 2021; Received in revised form 8 June 2021; Accepted 28 June 2021
Available online 2 July 2021

been reported to have high volumetric capacitances, such as $Nb_4C_3T_x$ at 1075 F/cm^3 and V_2CT_x at 1315 F/cm^3 [32]. Nb_2CT_x films have been employed to fabricate polarity reversible lithium ion capacitors, with a volumetric energy density of 50–70 Wh/L [33,34], and lithium ion battery anodes [35]. V_2CT_x has been investigated as an electrode for supercapacitors [32,36], lithium-ion [35,37], zinc-ion [38], and aluminum-ion [39] batteries. Ti_2CT_x has also been studied in electrodes for lithium and sodium ion batteries and supercapacitors [32,40,41]. M_2XT_x MXenes, compared with $M_3X_2T_x$, $M_4X_3T_x$, or $M_5X_4T_x$, have fewer atomic layers, but similar surface chemistry; thus they are expected to have a higher specific surface area and capacitance normalized by weight or volume. However, they have been less explored than $Ti_3C_2T_x$, partly because they are less chemically and electrochemically stable in aqueous environments, especially Ti_2CT_x and V_2CT_x [32,42,43]. Moreover, the electrochemical properties of solid-solution MXenes are less known, with M_2XT_x not reported thus far [26].

Herein, two series of niobium-containing solid-solution MXenes, $Ti_{2-y}Nb_yCT_x$ and $V_{2-y}Nb_yCT_x$ (y = 0.4, 0.8, 1.2, and 1.6), were synthesized, their electrochemical properties investigated and compared to corresponding single-metal MXenes (Ti_2CT_x, Nb_2CT_x, and V_2CT_x) (Fig. 1a). It is shown that their capacitive behavior and cycling stability can be tuned by modification of the M-site chemistry. As the niobium content is increased, the redox peak prominence decreases, while the cycling stability is enhanced. Moreover, niobium content is correlated with capacitance retention of $Ti_{2-y}Nb_yCT_x$: from less than 1% (y = 0, i.e., Ti_2CT_x) to 78% (y = 1.6, i.e., $Ti_{0.4}Nb_{1.6}CT_x$) after 20,000 cycles at 200 mV/s. Considering there are more than 100 predicted stoichiometric MXene compositions and a limitless number of solid solutions [29,44,45], this illustrates the viability of adjusting MXene electrochemical properties by tuning the M-site chemistry.

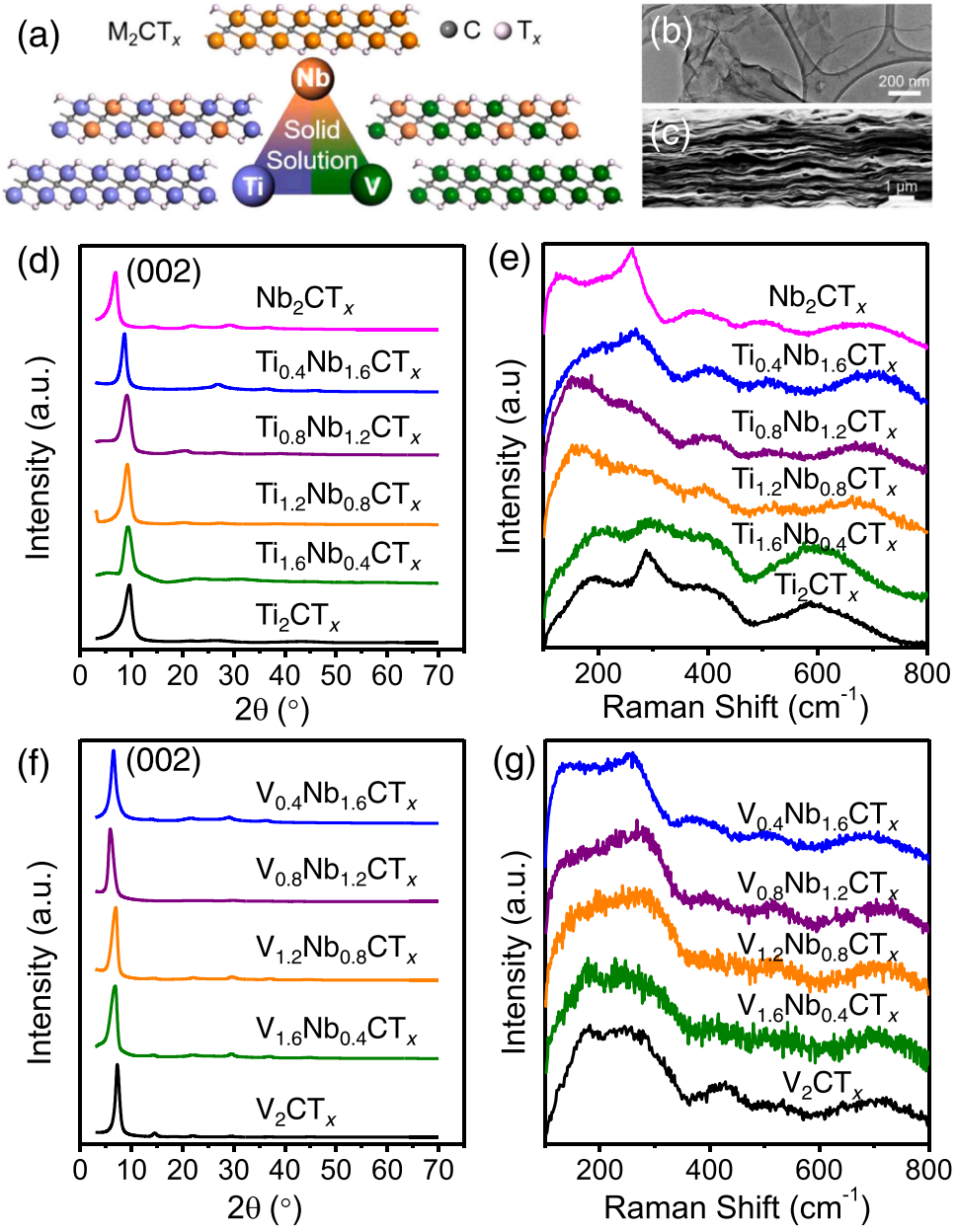

Fig. 1. (a) Schematic diagram of niobium-containing solid-solution MXenes ($Ti_{2-y}Nb_yCT_x$ and $V_{2-y}Nb_yCT_x$) with different discrete compositions. (b) Transmission electron microscopy (TEM) image of a $Ti_{1.6}Nb_{0.4}CT_x$ flake. (c) Scanning electron microscopy (SEM) image of the $Ti_{1.6}Nb_{0.4}CT_x$ film cross-section. X-ray diffraction (XRD) patterns (d) and Raman spectra (e) of $Ti_{2-y}Nb_yCT_x$, XRD patterns (f), and Raman spectra (g) of $V_{2-y}Nb_yCT_x$ with different Nb contents.

2. Results and discussion

Niobium-containing solid-solution MAX phases, $Ti_{2-y}Nb_yAlC$, $V_{2-y}Nb_yAlC$ (y = 0.4, 0.8, 1.2, and 1.6), and corresponding single-metal MAX phases, Ti_2AlC, V_2AlC, and Nb_2AlC, were synthesized using the previously described protocols [25]. XRD patterns of all MAX phases are shown in Fig. S1. It is important to note that only one MAX phase is present in each precursor mixture, indicating that these powders can be used to study each specific MXene chemistry [28]. After selective removal of Al from the MAX precursors and subsequent delamination, the corresponding MXenes were obtained. The elemental ratios are based on the initial MAX phase synthesis, assuming no transition metal ratio changes during the calcination or subsequent etching processes, as confirmed in other studies [29]. The Nb and Ti/V atoms in the MAX phases and MXenes are randomly distributed in M-layers. X-ray diffraction (XRD) patterns of $Ti_{2-y}Nb_yCT_x$ and $V_{2-y}Nb_yCT_x$ are shown in Fig. 1. The disappearance of higher order peaks with only (00 *l*) peaks remaining confirms that the Al layers were completely removed, delamination was successful, and no impurity phases remained in the films. The (002) peak positions and *d*-spacings of $Ti_{2-y}Nb_yCT_x$ and $V_{2-y}Nb_yCT_x$ are shown in Table 1. The *d*-spacings of V_2CT_x, $V_{2-y}Nb_yCT_x$ (y = 0.4, 0.8, 1.2, and 1.6), and Nb_2CT_x are larger than Ti_2CT_x and $Ti_{2-y}Nb_yCT_x$ (y = 0.4, 0.8, 1.2, and 1.6), which is due to the use of tetramethylammonium hydroxide intercalants during delamination, in contrast to Li ion intercalation for Ti_2CT_x and $Ti_{2-y}Nb_yCT_x$.

Fig. 1e shows the Raman spectra of $Ti_{2-y}Nb_yCT_x$. The collaborative vibration modes of Ti_2CT_x at around 287 cm^{-1}, 419 cm^{-1}, and 585 cm^{-1} should be attributed to Ti_2CO_2 [46], which are still apparent for $Ti_{1.6}Nb_{0.4}CT_x$ although their peak strength diminishes. However, for $Ti_{1.2}Nb_{0.8}CT_x$ and $Ti_{0.8}Nb_{1.2}CT_x$, these peaks are almost negligible probably due to the decreasing content of titanium in the MXenes. Similarly the strength of E_g modes of V_2CT_x at 181 cm^{-1} and 427 cm^{-1} decreases for $V_{1.6}Nb_{0.4}CT_x$ (Fig. 1g) [47]. For both, $Ti_{0.4}Nb_{1.6}CT_x$ and $V_{0.4}Nb_{1.6}CT_x$, the A_{1g} mode of Nb_2CT_x around 263 cm^{-1} becomes apparent when the niobium content increases to 80% [48].

To investigate the electrochemical properties of $Ti_{2-y}Nb_yCT_x$, their cyclic voltammetry (CV) curves were recorded at scan rates from 5 mV/s to 1000 mV/s, as shown in Fig. 2. A pair of redox peaks at −0.23 V/−0.22 V are observed on the CV curve of Ti_2CT_x at 5 mV/s scan rate. For $Ti_3C_2T_x$, the pseudocapacitance mainly originates from the following reversible surface redox reaction, which produces a prominent redox peak in its CV curve [49,50]:

$$Ti_3C_2O_2 + xH^+ + xe^- \rightleftharpoons Ti_3C_2O_{2-x}(OH)_x \quad (1)$$

The redox peaks of Ti_2CT_x may originate from a similar redox reaction, due to presence of Ti_2CO_2, which is supported by the Raman spectrum [46]:

$$Ti_2CO_2 + xH^+ + xe^- \rightleftharpoons Ti_2CO_{2-x}(OH)_x \quad (2)$$

At higher voltages, there is an additional pair of redox peaks at −0.08 V/−0.05 V, which is more prominent than the main redox peak. However, their magnitude decreases more rapidly with the increase of scan rate. Ti_2CT_x is prone to oxidation even in the preparation process [43,51]. To understand the influence of oxidation on its electrochemical behavior, anodic oxidation of Ti_2CT_x was performed through voltammetric cycling at a scan rate of 100 mV/s to 0.2 V vs Ag/AgCl [52], as shown in Fig. S2. During the first cycles of oxidation at 0.2 V, the right peak enlarges while the left side peak diminishes. Consequently, the redox peak pair on the right side is attributed to the electrochemically unstable species produced by the partial oxidation of Ti_2CT_x.

For all the samples containing titanium, from Ti_2CT_x to $Ti_{0.4}Nb_{1.6}CT_x$, a redox peak around 0.2 V is apparent at 5 mV/s, although the peak strength becomes less prominent as the Ti content decreases. There is no prominent redox peak for Nb_2CT_x in the CV curves (Fig. 2f), even at the lowest scan rate, which is similar to the electrochemical behavior of $Nb_4C_3T_x$ [53]. This is probably due to weaker ionic intercalation-deintercalation during the charge-discharge processes for Nb_2CT_x than Ti_2CT_x [18,54], which leads to a lower specific capacitance of Nb_2CT_x than Ti_2CT_x. With the increase of Nb content, the ionic intercalation-deintercalation might be inhibited, causing a trend of decrease in capacitance. This implies that the electrochemical behavior of solid-solution MXenes is tunable through the M-site chemistry.

From the CV curves, the specific capacitance values of Ti_2CT_x, $Ti_{1.6}Nb_{0.4}CT_x$, $Ti_{1.2}Nb_{0.8}CT_x$, $Ti_{0.8}Nb_{1.2}CT_x$, $Ti_{0.4}Nb_{1.6}CT_x$, and Nb_2CT_x at 5 mV/s are 490, 466, 404, 421, 363, and 245 F/g, respectively (Fig. 3a). When the scan rate is elevated to 1000 mV/s, the specific capacitance values decrease to 172, 240, 237, 175, 175, and 36 F/g, respectively, representing 35%, 52%, 59%, 42%, 48%, and 15% capacitance retention, respectively. The capacitance values of Ti_2CT_x, $Ti_{1.6}Nb_{0.4}CT_x$, $Ti_{1.2}Nb_{0.8}CT_x$, and $Ti_{0.8}Nb_{1.2}CT_x$ at 5 mV/s are all higher than $Ti_3C_2T_x$ hydrogel electrodes (380 F/g, with a rather similar mass loading of 1.2 mg/cm^2) [49]. This outstanding capacitance could be ascribed to thinner flakes of 2D $Ti_{2-y}Nb_yCT_x$, which have 3 atomic layers compared with 5 atomic layers of $Ti_3C_2T_x$, excluding the surface functional groups, with similar redox active titanium species on their surfaces. Our previous X-ray absorption studies showed similar oxidation state of Ti in both MXenes [55].

The CV curves of $Ti_{2-y}Nb_yCT_x$ compositions after every 2000 cycles at 200 mV/s are shown in Fig. S3 and their capacitance retentions are summarized in Fig. 3b. The capacitance of Ti_2CT_x diminishes quickly during cycling, dropping to negligible values after less than 3000 cycles. MXenes are prone to hydrolysis in water dispersion, the rate of which depends on the pH value and electrolyte composition, etc. [43,51,56] Hydrolysis can be minimized by adjusting the pH value or by the addition of antioxidants. Hydrolysis, leading to electrode degradation, may influence the cycling stability of the device. In the cycling test, the specific capacitance of Ti_2CT_x decreased to 23.68% and 11.2% of its initial value after 300 and 600 cycles, which corresponds to just 30 min and 60 min of CV cycling, respectively. Since colloidal Ti_2CT_x can be fully hydrolyzed within one day in oxygenated water, the fast decay of Ti_2CT_x capacitance should be attributed to its poor chemical stability in aqueous systems. Interestingly, by replacing only 20% of the Ti with Nb, the capacitance retention of $Ti_{1.6}Nb_{0.4}CT_x$ after 10,000 and 20,000 cycles is improved to 22% and 19%, respectively. As the Nb content increases to $Ti_{1.2}Nb_{0.8}CT_x$, $Ti_{0.8}Nb_{1.2}CT_x$, $Ti_{0.4}Nb_{1.6}CT_x$, the capacitance retention after 20,000 cycles increase to 30%, 60%, and 78%, respectively. The capacitance of the Nb_2CT_x electrode is increased to 118% of its initial value after 20,000 cycles due to the material "activation" and increase of accessible surface area in the interlayer space during the cycling process [57]. Overall, the capacitive behavior and cycling stability of $Ti_{2-y}Nb_yCT_x$ is directly related to the M-site chemistry.

Fig. S4 shows the electrochemical impedance spectroscopy (EIS) spectra of Ti_2CT_x, $Ti_{0.8}Nb_{1.2}CT_x$, and Nb_2CT_x before and after cycling. Before cycling, the charge transfer resistances of Ti_2CT_x, $Ti_{0.8}Nb_{1.2}CT_x$, and Nb_2CT_x, reflected by the radius of the semicircle on the Nyquist plot, are 0.3 Ω, 0.6 Ω, and 1.5 Ω, respectively. After cycling, they became 449.4 Ω, 4.0 Ω, and 0.65 Ω, respectively. The obvious increase of the charge transfer resistance of Ti_2CT_x suggests oxidation during cycling [58]. With the addition of Nb, the charge transfer resistance of the materials is stabilized during cycling. The low frequency slope also

Table 1
The (002) peak positions and *d*-spacings of $Ti_{2-y}Nb_yCT_x$ and $V_{2-y}Nb_yCT_x$.

			$Ti_{2-y}Nb_yCT_x$			
y	0	0.4	0.8	1.2	1.6	2
(002) Peak (°)	9.66	9.26	9.24	9.12	8.67	6.96
d-spacing (Å)	9.1	9.5	9.6	9.7	10.2	12.7
			$V_{2-y}Nb_yCT_x$			
y	0	0.4	0.8	1.2	1.6	/
(002) Peak (°)	7.23	6.84	6.99	5.85	6.51	/
d-spacing (Å)	12.2	12.9	12.6	15.1	13.6	/

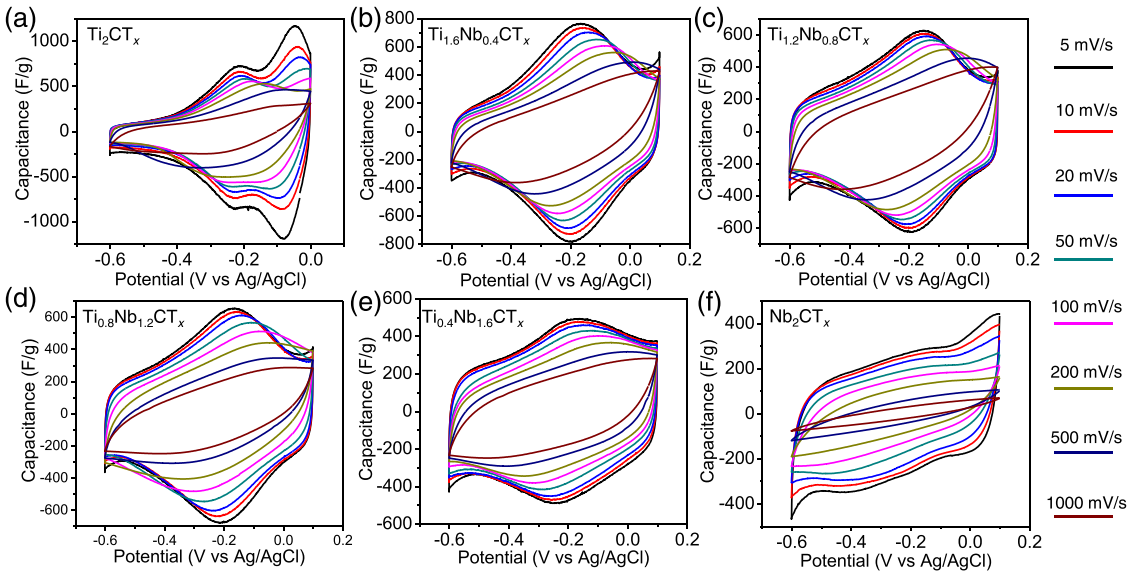

Fig. 2. Cyclic voltammetry (CV) curves of $Ti_{2-y}Nb_yCT_x$ (from (a) to (f): y = 0, 0.4, 0.8, 1.2, 1.6, and 2, respectively) obtained in 3 M H_2SO_4 electrolyte at scan rates from 5 mV/s to 1000 mV/s.

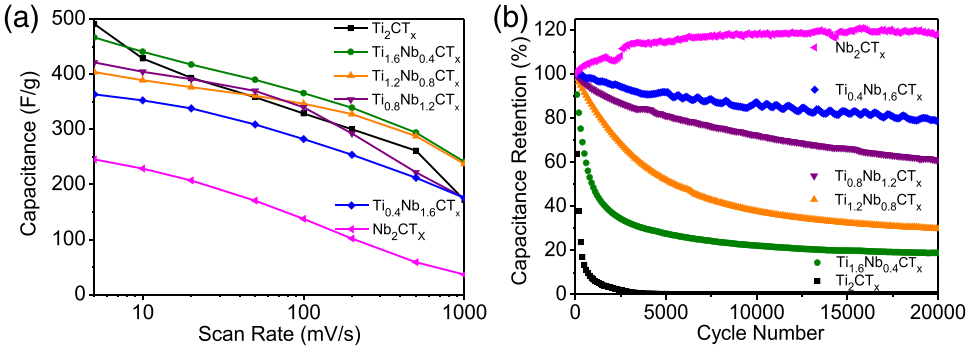

Fig. 3. (a) Specific capacitance of $Ti_{2-y}Nb_yCT_x$ as a function of scan rate. (b) Cycling stability of $Ti_{2-y}Nb_yCT_x$ at 200 mV/s.

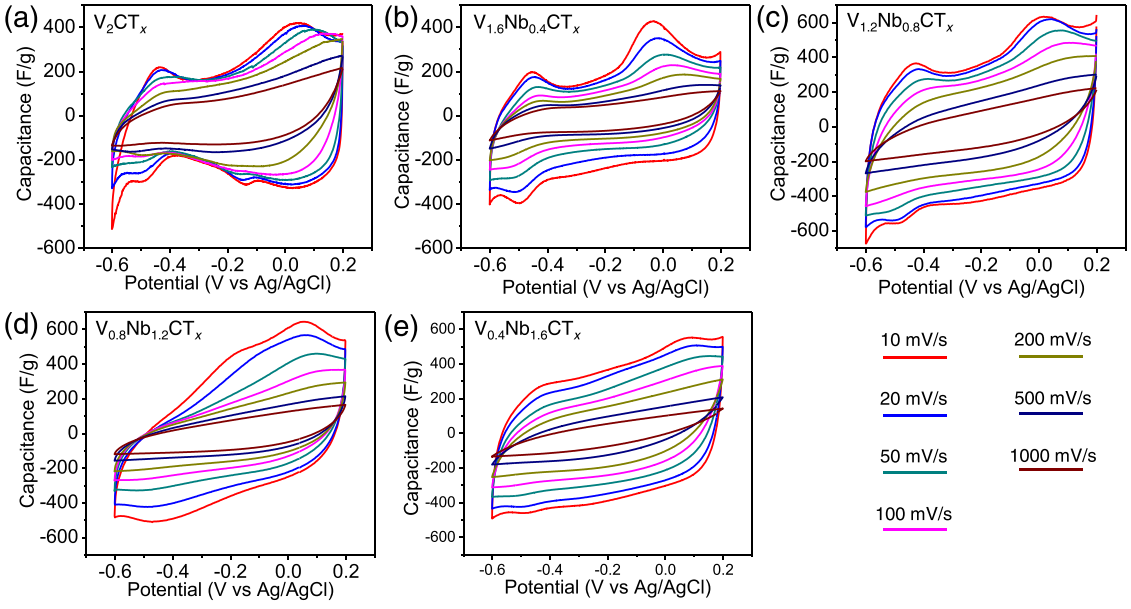

Fig. 4. CV curves of $V_{2-y}Nb_yCT_x$ obtained at different scan rates (from (a) to (e): y = 0, 0.4, 0.8, 1.2, and 1.6, respectively).

decreases, indicating higher Warburg impedance and a lower rate of ion diffusion after cycling [59]. The increase in charge transfer resistance for $Ti_{0.8}Nb_{1.2}CT_x$ is less than Ti_2CT_x, suggesting that its cycling stability is enhanced relative to Ti_2CT_x. The decrease of charge transfer resistance may explain the capacitance increase of Nb_2CT_x after cycling. The equivalent series resistance values of Ti_2CT_x and $Ti_{0.8}Nb_{1.2}CT_x$ are smaller than Nb_2CT_x, and do not change significantly after cycling.

The CV data of $V_{2-y}Nb_yCT_x$ were measured within the potential range of 0.2 V to −0.6 V versus Ag/AgCl, as shown in Fig. 4. There are two prominent redox peaks at around 0 V and −0.45 V in the CV curve of V_2CT_x. The position of the first peak coincides with earlier reports, although the second peak is absent since the potential range in that study was limited to 0.2 V to −0.4 V [32]. Similar to $Ti_{2-y}Nb_yCT_x$, the redox peak magnitude of $V_{2-y}Nb_yCT_x$ decreases as the Nb content increases. Anodic oxidation of $V_{1.6}Nb_{0.4}CT_x$ was conducted to understand the multiple redox peaks, as shown in Fig. S5. During cycling at a scan rate of 100 mV/s to 0.3 V vs Ag/AgCl [52], both peaks decrease simultaneously, in clear contrast with the behavior of Ti_2CT_x. Therefore, the appearance of two peaks is likely due to the multiple oxidation states of vanadium that can be achieved during the charge and discharge processes [60].

The capacitances of $V_{2-y}Nb_yCT_x$ at different scan rates are summarized in Fig. 5a. The capacitance of V_2CT_x at 10 mV/s is 240 F/g, not higher than Nb_2CT_x. No clear trend of capacitance change is observed in $V_{2-y}Nb_yCT_x$. The highest capacitance (410 F/g) is observed for $V_{1.2}Nb_{0.8}CT_x$ at 10 mV/s. The cycling stability of $V_{2-y}Nb_yCT_x$ was studied by cycling at 200 mV/s, and the CV curves after every 2000 cycles are shown in Fig. S6, with the capacitance retention plotted in Fig. 5b. After 20,000 cycles, V_2CT_x retains 26% of its initial capacitance. For $V_{1.6}Nb_{0.4}CT_x$, $V_{1.2}Nb_{0.8}CT_x$, $V_{0.8}Nb_{1.2}CT_x$, and $V_{0.4}Nb_{1.6}CT_x$, the capacitance retentions after 20,000 cycles were 27%, 33%, 61%, and 62%, respectively. Similar to $Ti_{2-y}Nb_yCT_x$, the cycling stability of materials in the $V_{2-y}Nb_yCT_x$ system increases with Nb content. Fig. S7 shows the Nyquist plots of V_2CT_x and $V_{0.8}Nb_{1.2}CT_x$ before and after cycling. Before cycling, the charge transfer resistance values of V_2CT_x and $V_{0.8}Nb_{1.2}CT_x$ were 0.85 Ω and 0.6 Ω, respectively. After cycling, they increased to 182 Ω and 21 Ω, respectively, suggesting oxide formation and lower stability of V_2CT_x compared to $V_{0.8}Nb_{1.2}CT_x$.

Both the redox peak area and the cycling stability of $Ti_{2-y}Nb_yCT_x$ and $V_{2-y}Nb_yCT_x$ show clear dependence on their composition. With low niobium contents, both $Ti_{2-y}Nb_yCT_x$ and $V_{2-y}Nb_yCT_x$ display prominent redox peaks in their CV curves. However, during cycling, the charge transfer resistances increase and the capacitances correspondingly decrease. Even though there were differences between the voltage windows used for different MXene compositions, that were needed to avoid oxidation during testing, one can confidently claim that the increase in Nb content leads to a decrease in the redox peak intensity and increase in cycling stability of M_2C MXenes. *In-situ* study of surface chemistry changes during charge and discharge should be conducted in the future to completely understand the mechanism of the charge storage processes in multi-element MXenes. A change in the local environment of transition metal atoms can affect their electrochemical potential and their redox and electrocatalytic ability. While limited to electrochemistry alone, this first study shows very significant variations of electrochemistry properties of solid-solution MXenes with changing amounts of M elements in the outer layers. This clearly shows a potential of designing MXene compositions to meet requirements of numerous electrochemical applications. With a dozen of early transition metals to choose from, 4 types of structures (not counting in- and out-of-plane ordered MXenes), plus a variety of surface terminations, guidance from computational studies will be needed to achieve efficient design of MXenes for future electrochemical applications. This is especially true, if more than 2 metals are mixed in M layers. However, the prospectives are truly exciting as an enormous compositional and structural space with a continuous change in parameters is now open to exploration.

3. Conclusions

In summary, two series of double-metal solid-solution MXenes, $Ti_{2-y}Nb_yCT_x$ and $V_{2-y}Nb_yCT_x$ (y = 0.4, 0.8, 1.2, and 1.6), were synthesized. It was shown that the capacitive properties and cycling stability of solid-solution MXenes directly depend on their composition. Moreover, for Nb-based M_2XT_x solid solutions, the redox peak intensity decreases while the cycling stability increases with the Nb content. The capacitance retention of $Ti_{2-y}Nb_yCT_x$ after 20,000 cycles increases from less than 1% for Ti_2CT_x to 78% for $Ti_{0.4}Nb_{1.6}CT_x$. The same trend is observed for $V_{2-y}Nb_yCT_x$. Since the number of MXene solid solutions is virtually limitless, the approach to controlling and optimizing the electrochemical properties of MXenes by combining transition metals in different proportions is certainly promising.

4. Material and methods

4.1. Material

Ti (99.5%, −325 mesh), V (99.5%, −325 mesh), Al (99.5%, −325 mesh), C (graphite, 99%, −325 mesh), and TiC (99.5%, typically 2 μm) powders were from Alfa Aesar, and Nb (99.99%, −325 mesh) was from Beantown Chemical for MAX phase synthesis. Lithium chloride (LiCl, 99%), hydrofluoric acid (HF, 48.5 −51%) and tetramethylammonium hydroxide (TMAOH, 25 wt%) were from Acros Organics, lithium fluoride (LiF, 98.5%) was from Alfa Aesar and hydrochloric acid (HCl, 36.5−38%) was from Fisher Chemical for the synthesis of MXene. All the chemicals were used as received without further purification.

4.2. Synthesis of MAX phases

For preparation of double-metal solid solution MAX phases, Ti, V, Nb, Al, and C powders (atomic ratio of Ti:Nb:Al:C and V:Nb:Al:C is 2-y:y:1.1:0.9, both for $Ti_{2-y}Nb_yAlC$ and $V_{2-y}Nb_yAlC$, y = 0, 0.4, 0.8, 1.2,

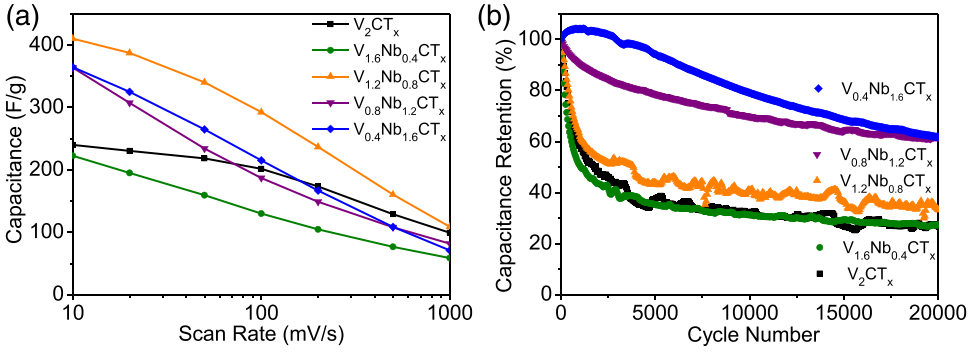

Fig. 5. (a) Specific capacitance of $V_{2-y}Nb_yCT_x$ as a function of scan rate. (b) Cycling stability of $V_{2-y}Nb_yCT_x$ at 200 mV/s.

1.6, and 2) were mixed with 10 mm zirconia balls in a 2:1 ball/powder ratio, placed in plastic jars and ball-milled at 50 rpm for 18 h. Subsequently, the precursor powder mixture was put in an alumina crucible and transferred into a high-temperature tube furnace (Carbolite Gero). Ar bubbling was used to purge the tube for 1 h before heating and kept throughout the whole synthesis process. The furnace was heated to 1550 ℃ at a rate of 3 ℃/min, held for 2 h and then cooled to room temperature at a rate of 3 ℃/min. Afterwards, they were milled with a TiN-coated milling bit and sieved to less than 75 μm.

4.3. Synthesis of MXenes

Synthesis of Ti_2CT_x. Ti_2CT_x was synthesized by the selective etching of Ti_2AlC with HF and HCl. First, 1 g of Ti_2AlC powder was added to a solution prepared by mixing 12 mL HCl, 2 mL HF, and 6 mL deionized (DI; 15 mΩ) water. Subsequently, the mixture was stirred for 24 h at room temperature, and then centrifuged at 3500 rpm for 2 min to remove the supernatant etching solution, followed by addition of DI water to redisperse the etched powders. This process was repeated until pH > 6. An aqueous LiCl solution with a concentration of 20 mg/mL was prepared and the centrifuge sediment was added into it. After being stirred for 4 h at room temperature, the mixture was centrifuged at 3500 rpm for 10 min and redispersed with DI water. The centrifugation/redispersion process was repeated until the supernatant became black after centrifugation. Afterwards, the black solution was centrifuged at 7500 rpm for 3 min and the final supernatant (colloidal solution of delaminated MXene flakes) was collected for the preparation of MXene films.

Synthesis of $Ti_{2-y}Nb_yCT_x$. The MILD method (LiF/HCl) was used to etch $Ti_{2-y}Nb_yAlC$ powders to produce $Ti_{2-y}Nb_yCT_x$ (y = 0.4, 0.8, 1.2, and 1.6). Typically, an etchant solution was prepared by dissolving LiF in a mixture of 5 mL DI water and 15 mL HCl. Subsequently, 1 g $Ti_{2-y}Nb_yAlC$ powder was put in the etchant solution slowly, followed by stirring at 35 °C for 48 h. After etching, the mixture was centrifuged at 3500 rpm for 2 min and then redispersed in DI water. The centrifuge/redispersion procedure was repeated several times until pH > 6. After redispersion of the sediment in DI water, the colloidal solution of delaminated $Ti_{2-y}Nb_yCT_x$ was obtained by centrifuging at 7500 rpm for 3 min.

Synthesis of $V_{2-y}Nb_yCT_x$. $V_{2-y}Nb_yCT_x$ (y = 0, 0.4, 0.8, 1.2, 1.6, and 2) was synthesized by selective etching of the precursor $V_{2-y}Nb_yAlC$ powders with HF. Typically, 1 g of MAX phase powder was introduced into 20 mL of 50 wt% HF and was stirred at 35 °C. After 48 h of etching, the etching solution was washed with DI water by centrifugation (3500 rpm, 2 min) several times until the pH of the solution exceeded 6, the sediment was collected and transferred into a solution with 0.5 g TMAOH dissolved in 20 mL DI water, followed by 12 h of stirring at room temperature. The mixture solution was washed through repeated centrifugation at 9000 rpm for 10 min, then redispered; this process was repeated until the pH dropped below 8. Finally, after the solution was centrifuged at 3500 rpm for 10 min, the black supernatant was collected as delaminated MXene aqueous dispersion (colloidal solution).

4.4. Characterization

Freestanding MXene films were obtained by vacuum-assisted filtration of the as-prepared MXene dispersion on a microporous membrane (3501 Coated PP, 25 μm, Celgard LLC), followed by drying in a vacuum oven. The concentration of the MXene dispersion was derived from the weight of the film and the filtered volume of the dispersion. The morphology and structure of MXene were observed with scanning electron microscopy (SEM; Zeiss Supra 50VP), and transmission electron microscopy (TEM; F-30, FEI-Tecnai). Raman spectra were recorded with a Renishaw (UK) Raman InVia confocal microscope, with a laser excitation of 633 nm, grating 1200 gr/mm and 5% laser power. XRD patterns were measured with Ni-filtered Cu K_α radiation ($\lambda = 1.54$ Å; Miniflex, Rigaku, Japan) operated at 40 kV and 15 mA with a step scan of 0.03° and holding time of 0.5 s.

4.5. Electrochemical measurements

Freestanding MXene films of 4 cm in diameter were prepared though vacuum-assisted filtration of MXene colloidal solution with concentration around 1 mg/mL to make samples with average weight of ~13 mg. A 3 mm-diameter MXene disk was cut out and employed as the working electrode, a 3 mm-diameter overcapacitive activated carbon film (95% YP50, Kuraray, Japan; 5% polytetrafluoroethylene, Sigma-Aldrich) and Ag/AgCl in 3.5 M KCl were used as the counter electrode and reference electrode, respectively. 3 M H_2SO_4 was used as electrolyte. Electrochemical measurements were performed in a Swagelok cell using a 3-electrode configuration. The detailed mass loading for each sample is shown in the Supplementary Data. Cyclic voltammetry (CV), galvanostatic cycling, and electrochemical impedance spectroscopy (EIS) experiments were performed at room temperature on a Bio-Logic (France) VMP3 electrochemical workstation.

CRediT authorship contribution statement

Likui Wang: Conceptualization, Experiment, Analysis, Drafting & editing, Funding acquisition. **Meikang Han**: Conceptualization, Experiment, Analysis, Review & editing. **Christopher E. Shuck**: Experiment, Analysis, Review & editing. **Xuehang Wang**: Analysis, Review & editing. **Yury Gogotsi**: Supervision, Conceptualization, Review & editing, Project administration, Funding acquisition.

Declaration of Competing Interest

The authors declare that they have no known competing financial interests or personal relationships that could have appeared to influence the work reported in this paper.

Acknowledgments

Research on MXene solid solutions at Drexel was supported by the US National Science Foundation (Ceramics Program) grant DMR-2041050. Likui Wang was sponsored by the China Scholarship Council (CSC) and The National Natural Science Foundation of China (51302109). XRD, SEM, and TEM analyses were performed using instruments in the Materials Characterization Core at Drexel University.

Appendix A. Supporting information

Supplementary data associated with this article can be found in the online version at doi:10.1016/j.nanoen.2021.106308.

References

[1] P. Simon, Y. Gogotsi, Materials for electrochemical capacitors, Nat. Mater. 7 (2008) 845–854, https://doi.org/10.1038/nmat2297.
[2] P. Simon, Y. Gogotsi, B. Dunn, Where do batteries end and supercapacitors begin? Science 343 (2014) 1210–1211, https://doi.org/10.1126/science.1249625.
[3] P. Simon, Y. Gogotsi, Perspectives for electrochemical capacitors and related devices, Nat. Mater. 19 (2020) 1151–1163, https://doi.org/10.1038/s41563-020-0747-z.
[4] B.E. Conway, Electrochemical Supercapacitors, Scientific Fundamentals and Technological Applications, Springer, US, 1999.
[5] W. Sugimoto, H. Iwata, K. Yokoshima, Y. Murakami, Y. Takasu, Proton and electron conductivity in hydrous ruthenium oxides evaluated by electrochemical impedance spectroscopy: the origin of large capacitance, J. Phys. Chem. B 109 (2005) 7330–7338, https://doi.org/10.1021/jp044252o.
[6] C. Sassoye, C. Laberty, H. Le Khanh, S. Cassaignon, C. Boissiere, M. Antonietti, C. Sanchez, Block-copolymer-templated synthesis of electroactive RuO_2-based mesoporous thin films, Adv. Funct. Mater. 19 (2009) 1922–1929, https://doi.org/10.1002/adfm.200801831.

[7] J.P. Zheng, P.J. Cygan, T.R. Jow, Hydrous ruthenium oxide as an electrode material for electrochemical capacitors, J. Electrochem. Soc. 142 (1995) 2699–2703, https://doi.org/10.1149/1.2050077.

[8] M. Toupin, T. Brousse, D. Belanger, Charge storage mechanism of MnO_2 electrode used in aqueous electrochemical capacitor, Chem. Mater. 16 (2004) 3184–3190, https://doi.org/10.1021/cm049649j.

[9] J. Come, V. Augustyn, J.W. Kim, P. Rozier, P.-L. Taberna, P. Gogotsi, J.W. Long, B. Dunn, P. Simon, Electrochemical kinetics of nanostructured Nb_2O_5 electrodes, J. Electrochem. Soc. 161 (2014) A718–A725, https://doi.org/10.1149/2.040405jes.

[10] V. Augustyn, J. Come, M.A. Lowe, J.W. Kim, P.-L. Taberna, S.H. Tolbert, H. D. Abruna, P. Simon, B. Dunn, High-rate electrochemical energy storage through Li^+ intercalation pseudocapacitance, Nat. Mater. 12 (2013) 518–522, https://doi.org/10.1038/nmat3601.

[11] X. Zhou, H. Chen, D. Shu, C. He, J. Nan, Study on the electrochemical behavior of vanadium nitride as a promising supercapacitor material, J. Phys. Chem. Solids 70 (2009) 495–500, https://doi.org/10.1016/j.jpcs.2008.12.004.

[12] A.M. Glushenkov, D. Hulicova-Jurcakova, D. Llewellyn, G.Q. Lu, Y. Chen, Structure and capacitive properties of porous nanocrystalline VN prepared by temperature-programmed ammonia reduction of V_2O_5, Chem. Mater. 22 (2010) 914–921, https://doi.org/10.1021/cm901729x.

[13] M.-S. Balogun, W. Qiu, W. Wang, P. Fang, X. Lu, Y. Tong, Recent advances in metal nitrides as high-performance electrode materials for energy storage devices, J. Mater. Chem. A 3 (2015) 1364–1387, https://doi.org/10.1039/C4TA05565A.

[14] H. Wang, J. Li, K. Li, Y. Lin, J. Chen, L. Gao, V. Nicolosi, X. Xiao, J.-M. Lee, Transition metal nitrides for electrochemical energy applications, Chem. Soc. Rev. 50 (2021) 1354–1390, https://doi.org/10.1039/D0CS00415D.

[15] G. Wang, L. Zhang, J. Zhang, A review of electrode materials for electrochemical supercapacitors, Chem. Soc. Rev. 41 (2012) 797–828, https://doi.org/10.1039/c1cs15060j.

[16] V. Augustyn, P. Simon, B. Dunn, Pseudocapacitive oxide materials for high-rate electrochemical energy storage, Energy Environ. Sci. 7 (2014) 1597–1614, https://doi.org/10.1039/c3ee44164d.

[17] B. Anasori, M.R. Lukatskaya, Y. Gogotsi, 2D metal carbides and nitrides (MXenes) for energy storage, Nat. Rev. Mater. 2 (2017) 17, https://doi.org/10.1038/natrevmats.2016.98.

[18] X. Wang, T.S. Mathis, K. Li, Z. Lin, L. Vlcek, T. Torita, N.C. Osti, C. Hatter, P. Urbankowski, A. Sarycheva, M. Tyagi, E. Mamontov, P. Simon, Y. Gogotsi, Influences from solvents on charge storage in titanium carbide MXenes, Nat. Energy 4 (2019) 241–248, https://doi.org/10.1038/s41560-019-0339-9.

[19] G. Deysher, C.E. Shuck, K. Hantanasirisakul, N.C. Frey, A.C. Foucher, K. Maleski, A. Sarycheva, V.B. Shenoy, E.A. Stach, B. Anasori, Y. Gogotsi, Synthesis of Mo_4VAlC_4 MAX phase and two-dimensional Mo_4VC_4 MXene with five atomic layers of transition metals, ACS Nano 14 (2020) 204–217, https://doi.org/10.1021/acsnano.9b07708.

[20] M. Naguib, M. Kurtoglu, V. Presser, J. Lu, J. Niu, M. Heon, L. Hultman, Y. Gogotsi, M.W. Barsoum, Two-dimensional nanocrystals produced by exfoliation of Ti_3AlC_2, Adv. Mater. 23 (2011) 4248–4253, https://doi.org/10.1002/adma.201102306.

[21] M. Sokol, V. Natu, S. Kota, M.W. Barsoum, On the chemical diversity of the MAX phases, Trends Chem. 1 (2019) 210–223, https://doi.org/10.1016/j.trechm.2019.02.016.

[22] C. Zhang, Y.L. Ma, X.T. Zhang, S. Abdolhosseinzadeh, H.W. Sheng, W. Lan, A. Pakdel, J. Heier, F. Nuesch, Two-dimensional transition metal carbides and nitrides (MXenes): synthesis, properties, and electrochemical energy storage applications, Energy Environ. Mater. 3 (2020) 29–55, https://doi.org/10.1002/eem2.12058.

[23] C.E. Shuck, Y. Gogotsi, Taking MXenes from the lab to commercial products, Chem. Eng. J. 401 (2020), 125786, https://doi.org/10.1016/j.cej.2020.125786.

[24] C.E. Shuck, A. Sarycheva, M. Anayee, A. Levitt, Y. Zhu, S. Uzun, V. Balitskiy, V. Zahorodna, O. Gogotsi, Y. Gogotsi, Scalable synthesis of $Ti_3C_2T_x$ MXene, Adv. Eng. Mater. 22 (2020), 1901241, https://doi.org/10.1002/adem.201901241.

[25] M. Han, C.E. Shuck, R. Rakhmanov, D. Parchment, B. Anasori, C.M. Koo, G. Friedman, Y. Gogotsi, Beyond $Ti_3C_2T_x$: MXenes for electromagnetic interference shielding, in: ACS Nano, 14, 2020, pp. 5008–5016, https://doi.org/10.1021/acsnano.0c01312.

[26] D. Pinto, B. Anasori, H. Avireddy, C.E. Shuck, K. Hantanasirisakul, G. Deysher, J. R. Morante, W. Porzio, H.N. Alshareef, Y. Gogotsi, Synthesis and electrochemical properties of 2D molybdenum vanadium carbides-solid solution MXenes, J. Mater. Chem. A 8 (2020) 8957–8968, https://doi.org/10.1039/d0ta01798a.

[27] B. Ahmed, A.E. Ghazaly, J. Rosen, *i*-MXenes for energy storage and catalysis, Adv. Funct. Mater. 30 (2020), 2000894, https://doi.org/10.1002/adfm.202000894.

[28] M. Shekhirev, C.E. Shuck, A. Sarycheva, Y. Gogotsi, Characterization of MXenes at every step, from their precursors to single flakes and assembled films, Prog. Mater. Sci. (2020), 100757, https://doi.org/10.1016/j.pmatsci.2020.100757.

[29] M. Han, K. Maleski, C.E. Shuck, Y. Yang, J.T. Glazar, A.C. Foucher, K. Hantanasirisakul, A. Sarycheva, N.C. Frey, S.J. May, V.B. Shenoy, E.A. Stach, Y. Gogotsi, Tailoring electronic and optical properties of MXenes through forming solid solutions, J. Am. Chem. Soc. 142 (2020) 19110–19118, https://doi.org/10.1021/jacs.0c07395.

[30] M. Ghidiu, M.R. Lukatskaya, M.-Q. Zhao, Y. Gogotsi, M.W. Barsoum, Conductive two-dimensional titanium carbide 'clay' with high volumetric capacitance, Nature 516 (2014) 78–81, https://doi.org/10.1038/nature13970.

[31] J. Zhang, N. Kong, S. Uzun, A. Levitt, S. Seyedin, P.A. Lynch, S. Qin, M. Han, W. Yang, J. Liu, X. Wang, Y. Gogotsi, J.M. Razal, Scalable manufacturing of free-standing, strong $Ti_3C_2T_x$ MXene films with outstanding conductivity, Adv. Mater. 32 (2020), 2001093, https://doi.org/10.1002/adma.202001093.

[32] A. VahidMohammadi, M. Mojtabavi, N.M. Caffrey, M. Wanunu, M. Beidaghi, Assembling 2D MXenes into highly stable pseudocapacitive electrodes with high power and energy densities, Adv. Mater. 31 (2019), 1806931, https://doi.org/10.1002/adma.201806931.

[33] A. Byeon, A.M. Glushenkov, B. Anasori, P. Urbankowski, J.W. Li, B.W. Byles, B. Blake, K.L. Van Aken, S. Kota, E. Pomerantseva, J.W. Lee, Y. Chen, Y. Gogotsi, Lithium-ion capacitors with 2D Nb_2CT_x (MXene)-carbon nanotube electrodes, J. Power Sources 326 (2016) 686–694, https://doi.org/10.1016/j.jpowsour.2016.03.066.

[34] O. Mashtalir, M.R. Lukatskaya, M.-Q. Zhao, M.W. Barsoum, Y. Gogotsi, Amine-assisted delamination of Nb_2C MXene for Li-ion energy storage devices, Adv. Mater. 27 (2015) 3501–3506, https://doi.org/10.1002/adma.201500604.

[35] M. Naguib, J. Halim, J. Lu, K.M. Cook, L. Hultman, Y. Gogotsi, M.W. Barsoum, New two-dimensional niobium and vanadium carbides as promising materials for Li-ion batteries, J. Am. Chem. Soc. 135 (2013) 15966–15969, https://doi.org/10.1021/ja405735d.

[36] C. Wang, S. Wei, S. Chen, D. Cao, L. Song, Delaminating vanadium carbides for zinc-ion storage: Hydrate precipitation and H^+/Zn^{2+} co-action mechanism, Small Methods 3 (2019), 1900495, https://doi.org/10.1002/smtd.201900495.

[37] F. Liu, J. Zhou, S. Wang, B. Wang, C. Shen, L. Wang, Q. Hu, Q. Huang, A. Zhou, Preparation of high-purity V_2C MXene and electrochemical properties as Li-ion batteries, J. Electrochem. Soc. 164 (2017) A709–A713, https://doi.org/10.1149/2.0641704jes.

[38] R. Venkatkarthick, N. Rodthongkum, X.Y. Zhang, S.M. Wang, P. Pattananuwat, Y. S. Zhao, R.P. Liu, J.Q. Qin, Vanadium-based oxide on two-dimensional vanadium carbide MXene (V_2O_x@V_2CT_x) as cathode for rechargeable aqueous zinc-ion batteries, ACS Appl. Energy Mater. 3 (2020) 4677–4689, https://doi.org/10.1021/acsaem.0c00309.

[39] A. VahidMohammadi, A. Hadjikhani, S. Shahbazmohamadi, M. Beidaghi, Two-dimensional vanadium carbide (MXene) as a high-capacity cathode material for rechargeable aluminum batteries, ACS Nano 11 (2017) 11135–11144, https://doi.org/10.1021/acsnano.7b05350.

[40] J. Fu, J. Yun, S. Wu, L. Li, L. Yu, K.H. Kim, Architecturally robust graphene-encapsulated MXene Ti_2CT_x@polyaniline composite for high-performance pouch-type asymmetric supercapacitor, ACS Appl. Mater. Interfaces 10 (2018) 34212–34221, https://doi.org/10.1021/acsami.8b10195.

[41] Y.R. Li, N. Li, S.J. Zhao, J. Fan, J.J. Kai, Strain-tunable electronic properties and lithium storage of 2D transition metal carbide (MXene) Ti_2CO_2 as a flexible electrode, J. Mater. Chem. A 8 (2020) 760–769, https://doi.org/10.1039/c9ta09185h.

[42] C.J. Zhang, S. Pinilla, N. McEyoy, C.P. Cullen, B. Anasori, E. Long, S.-H. Park, A. Seral-Ascaso, A. Shmeliov, D. Krishnan, C. Morant, X. Liu, G.S. Duesberg, Y. Gogotsi, V. Nicolosi, Oxidation stability of colloidal two-dimensional titanium carbides (MXenes), Chem. Mater. 29 (2017) 4848–4856, https://doi.org/10.1021/acs.chemmater.7b00745.

[43] S.H. Huang, V.N. Mochalin, Hydrolysis of 2D transition-metal carbides (MXenes) in colloidal solutions, Inorg. Chem. 58 (2019) 1958–1966, https://doi.org/10.1021/acs.inorgchem.8b02890.

[44] Y. Gogotsi, B. Anasori, The rise of MXenes, ACS Nano 13 (2019) 8491–8494, https://doi.org/10.1021/acsnano.9b06394.

[45] M. Dahlqvist, J. Rosen, Predictive theoretical screening of phase stability for chemical order and disorder in quaternary 312 and 413 MAX phases, Nanoscale 12 (2020) 785–794, https://doi.org/10.1039/c9nr08675g.

[46] U. Yorulmaz, A. Ozden, N.K. Perkgoz, F. Ay, C. Sevik, Vibrational and mechanical properties of single layer MXene structures: a first-principles investigation, Nanotechnology 27 (2016) 10, https://doi.org/10.1088/0957-4484/27/33/335702.

[47] A. Champagne, L. Shi, T. Ouisse, B. Hackens, J.-C. Charlier, Electronic and vibrational properties of V_2C-based MXenes: from experiments to first-principles modeling, Phys. Rev. B 97 (2018), 115439, https://doi.org/10.1103/PhysRevB.97.115439.

[48] Y. Luo, C. Cheng, H.-J. Chen, K. Liu, X.-L. Zhou, Systematic investigations of the electron, phonon and elastic properties of monolayer M2C (M = V, Nb, Ta) by first-principles calculations, J. Phys.: Condens. Matter 31 (2019), 405703, https://doi.org/10.1088/1361-648x/ab2847.

[49] M.R. Lukatskaya, S. Kota, Z. Lin, M.-Q. Zhao, N. Shpigel, M.D. Levi, J. Halim, P.-L. Taberna, M.W. Barsoum, P. Simon, Y. Gogotsi, Ultra-high-rate pseudocapacitive energy storage in two-dimensional transition metal carbides, Nat. Energy 2 (2017) 17105, https://doi.org/10.1038/nenergy.2017.105.

[50] M. Hu, Z. Li, T. Hu, S. Zhu, C. Zhang, X. Wang, High-capacitance mechanism for $Ti_3C_2T_x$ MXene by in situ electrochemical Raman spectroscopy investigation, ACS Nano 10 (2016) 11344–11350, https://doi.org/10.1021/acsnano.6b06597.

[51] C.J. Zhang, S. Pinilla, N. McEvoy, C.P. Cullen, B. Anasori, E. Long, S.-H. Park, A. Seral-Ascaso, A. Shmeliov, D. Krishnan, C. Morant, X. Liu, G.S. Duesberg, Y. Gogotsi, V. Nicolosi, Oxidation stability of colloidal two-dimensional titanium carbides (MXenes), Chem. Mater. 29 (2017) 4848–4856, https://doi.org/10.1021/acs.chemmater.7b00745.

[52] J. Tang, T.S. Mathis, N. Kurra, A. Sarycheva, X. Xiao, M.N. Hedhili, Q. Jiang, H. N. Alshareef, B. Xu, F. Pan, Y. Gogotsi, Tuning the electrochemical performance of titanium carbide MXene by controllable in situ anodic oxidation, Angew. Chem. Int. Ed. 58 (2019) 17849–17855, https://doi.org/10.1002/anie.201911604.

[53] S. Zhao, C. Chen, X. Zhao, X. Chu, F. Du, G. Chen, Y. Gogotsi, Y. Gao, Y. Dall'Agnese, Flexible $Nb_4C_3T_x$ film with large interlayer spacing for high-performance supercapacitors, Adv. Funct. Mater. 30 (2020), 2000815, https://doi.org/10.1002/adfm.202000815.

[54] A. Sugahara, Y. Ando, S. Kajiyama, K. Yazawa, K. Gotoh, M. Otani, M. Okubo, A. Yamada, Negative dielectric constant of water confined in nanosheets, Nat. Commun. 10 (2019) 850, https://doi.org/10.1038/s41467-019-08789-8.
[55] Y.Z. Yang, K. Hantanasirisakul, N.C. Frey, B. Anasori, R.J. Green, P.C. Rogge, I. Waluyo, A. Hunt, P. Shafer, E. Arenholz, V.B. Shenoy, Y. Gogotsi, S.J. May, Distinguishing electronic contributions of surface and sub-surface transition metal atoms in Ti-based MXenes, 2D Mater. 7 (2020), 025015, https://doi.org/10.1088/2053-1583/ab68e7.
[56] X. Zhao, A. Vashisth, J.W. Blivin, Z. Tan, D.E. Holta, V. Kotasthane, S.A. Shah, T. Habib, S. Liu, J.L. Lutkenhaus, M. Radovic, M.J. Green, pH nanosheet concentration, and antioxidant affect the oxidation of $Ti_3C_2T_x$ and Ti_2CT_x MXene dispersions, Adv. Mater. Interfaces 7 (2020), 2000845, https://doi.org/10.1002/admi.202000845.
[57] Y.-Y. Peng, B. Akuzum, N. Kurra, M.-Q. Zhao, M. Alhabe, B. Anasori, E.C. Kumbur, H.N. Alshareef, M.-D. Ger, Y. Gogotsi, All-MXene (2D titanium carbide) solid-state microsupercapacitors for on-chip energy storage, Energy Environ. Sci. 9 (2016) 2847–2854, https://doi.org/10.1039/c6ee01717g.
[58] D. Jung, M. Muni, G. Marin, R. Ramachandran, M.F. El-Kady, T. Balandin, R. B. Kaner, A.M. Spokoyny, Enhancing cycling stability of tungsten oxide supercapacitor electrodes via a boron cluster-based molecular cross-linking approach, J. Mater. Chem. A 8 (2020) 18015–18023, https://doi.org/10.1039/D0TA05915C.
[59] R. Kötz, M. Carlen, Principles and applications of electrochemical capacitors, Electrochim. Acta 45 (2000) 2483–2498, https://doi.org/10.1016/S0013-4686(00)00354-6.
[60] G. Silversmit, D. Depla, H. Poelman, G.B. Marin, R. De Gryse, Determination of the V2p XPS binding energies for different vanadium oxidation states (V^{5+} to V^{0+}), J. Electron. Spectrosc. Relat. Phenom. 135 (2004) 167–175, https://doi.org/10.1016/j.elspec.2004.03.004.

Likui Wang is an associate professor at the School of Chemical and Materials Engineering, Jiangnan University. He obtained his Ph.D. from the National University of Singapore in 2009 and joined the Essilor Singapore R&D Center subsequently. In 2012, he started to work at Jiangnan University and was a visiting scholar at A.J. Drexel Nanomaterials Institute, Drexel University from Oct 2018 to Oct 2019. His current research interests include the synthesis of nanostructured conducting polymers, 2D transition metal carbides/nitrides and their applications on electrochemical energy storage and conversion.

Meikang Han is a postdoctoral researcher at A.J. Drexel Nanomaterials Institute and the Department of Materials Science and Engineering at Drexel University. He received his Ph. D. degree in Materials Science from Northwestern Polytechnical University, China in 2018. His research interests include the synthesis of two-dimensional nanomaterials and their electromagnetic applications (electromagnetic interference shielding, wireless communications, wearable devices, *etc*.).

Christopher E. Shuck is a postdoctoral fellow at the A.J. Drexel Nanomaterials Institute, Drexel University. He received his Ph.D. in 2018 from the University of Notre Dame in Chemical and Biomolecular Engineering, and B.S.E. in 2013 from Princeton University in Chemical and Biological Engineering. His research interests include chemical kinetics, materials synthesis, and 2D materials; he is broadly focused on the relationship between how materials are synthesized and their resulting properties.

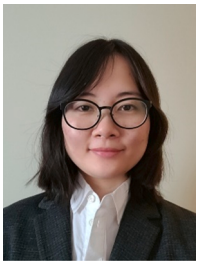

Xuehang Wang is currently an assistant professor at the Department of Radiation Science and Technology at Delft University of Technology. She received her Ph.D. in chemical engineering from the Norwegian University of Science and Technology in 2016, and was a postdoctoral researcher at A.J. Drexel Nanomaterials Institute, Drexel University, from 2017 to 2020. Her research interests are in the charge mechanism of energy storage devices, especially the electrolyte transportation at electrode-electrolyte interfaces of 2D MXenes and various carbon materials.

Dr Yury Gogotsi received MS (1984) and PhD (1986) degrees from Kiev Polytechnic and a DSc degree from the Ukrainian Academy of Sciences in 1995. Now he is Charles T. and Ruth M. Bach Distinguished University Professor of Materials Science and Engineering at Drexel University. He also holds appointments in the Departments of Chemistry and Mechanical Engineering and Mechanics and serves as Director of the A.J. Drexel Nanomaterials Institute. His research interests include various nanostructured carbons and other nanomaterials, such as two-dimensional transition metal carbides, nitrides/carbonitrides (MXenes) and their applications.